NANO LETTERS

Letter

pubs.acs.org/NanoLett

Electrical and Optical Characterization of Surface Passivation in GaAs Nanowires

Chia-Chi Chang,[†,∥] Chun-Yung Chi,[‡,∥] Maoqing Yao,[‡,∥] Ningfeng Huang,[‡,∥] Chun-Chung Chen,[‡,∥] Jesse Theiss,[‡,∥] Adam W. Bushmaker,[⊥] Stephen LaLumondiere,[⊥] Ting-Wei Yeh,[§,∥] Michelle L. Povinelli,[‡,∥] Chongwu Zhou,[‡,∥] P. Daniel Dapkus,[‡,∥] and Stephen B. Cronin*[,†,‡,∥]

[†]Department of Physics, [‡]Department of Electrical Engineering, [§]Department of Chemical Engineering and Materials Science, and [∥]Center for Energy Nanoscience, University of Southern California, Los Angeles, California 90089, United States

[⊥]The Aerospace Corporation, Los Angeles, California 90009-2957, United States

Supporting Information

ABSTRACT: We report a systematic study of carrier dynamics in $Al_xGa_{1-x}As$-passivated GaAs nanowires. With passivation, the minority carrier diffusion length (L_{diff}) increases from 30 to 180 nm, as measured by electron beam induced current (EBIC) mapping, and the photoluminescence (PL) lifetime increases from sub-60 ps to 1.3 ns. A 48-fold enhancement in the continuous-wave PL intensity is observed on the same individual nanowire with and without the $Al_xGa_{1-x}As$ passivation layer, indicating a significant reduction in surface recombination. These results indicate that, in passivated nanowires, the minority carrier lifetime is not limited by twin stacking faults. From the PL lifetime and minority carrier diffusion length, we estimate the surface recombination velocity (SRV) to range from 1.7×10^3 to 1.1×10^4 cm·s^{-1}, and the minority carrier mobility μ is estimated to lie in the range from 10.3 to 67.5 cm^2 V^{-1} s^{-1} for the passivated nanowires.

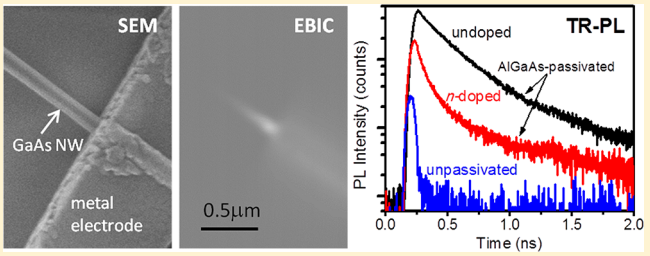

KEYWORDS: *MOCVD, EBIC, TR-PL, GaAs, surface passivation, selective area growth*

GaAs is one of the most widely used semiconductors, second to silicon, with applications in fast electronics, infrared LEDs,[1] and high-efficiency solar cells.[2] However, GaAs suffers from pronounced effects associated with its surface states, which has prevented GaAs metal-oxide-semiconductor field-effect transistors (MOSFET) from becoming a viable technology. This problem is also reflected in GaAs' extremely high surface recombination velocity (10^6 cm/s), which is 3 orders of magnitude higher than most other III−V semiconductors.[3,4] The surface depletion effect in GaAs is exacerbated in nanostructures with high surface-to-volume ratios. For example, semi-insulating electrical behavior was observed in highly doped GaAs nanowires without surface treatment.[5] Ammonium polysulfide $(NH_4)_2S_x$ has been used to passivate the surfaces of III−V semiconductors with covalently bonded sulfur atoms.[6,7] However, sulfur-passivation only provides short-term surface stability. Passivating GaAs nanowires with a wide band gap semiconductor such as $Al_xGa_{1-x}As$ provides long-term surface stability.[8−12]

Here, we present a systematic study of $Al_xGa_{1-x}As$-passivated GaAs nanowires using spatial mapping of Raman and photoluminescence (PL) spectroscopy, time-resolved photoluminescence (TRPL) spectroscopy, and electron beam induced current (EBIC) mapping. These measurements directly probe the minority carrier diffusion length and lifetime in these nanowires. The surface recombination velocity and carrier mobility are also calculated on the basis of the experimental results.

As mentioned above, the problems associated with surface states and surface depletion are more severe in GaAs nanowires because of their high surface−volume ratios. In moderately doped nanowires, the depletion region will consist of a cylindrical ring with a conducting channel in the middle of the nanowire. If the doping is too low, however, the entire nanowire cross section will be depleted, and therefore insulating. Figure 1 shows the free carrier density plotted as a function of the dopant impurity concentration for several nanowire diameters calculated by solving the Poisson equation with Fermi−Dirac statistics, assuming midgap pinning of the surface Fermi level. For a 100 nm diameter nanowire, doping concentrations below 10^{17} cm^{-3} yield completely depleted nanowires. Because of these surface states, dopant impurity concentrations above approximately 7×10^{17} cm^{-3} are needed in order to generate a significant amount of free carriers in this material. There are two ways to mitigate this problem. First, the nanowires can be heavily doped, $N_I \geq 10^{18}$ cm^{-3}, or the GaAs surface can be passivated with a wider bandgap semiconductor, such as $Al_xGa_{1-x}As$ or GaP.

Received: April 12, 2012
Revised: June 21, 2012

   dx.doi.org/10.1021/nl301391h | *Nano Lett.* XXXX, XXX, XXX−XXX

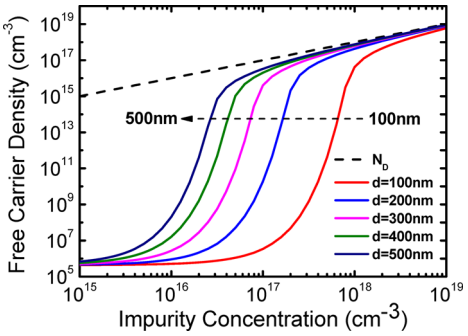

Figure 1. The calculated free carrier density plotted as a function of dopant impurity concentration for GaAs nanowires with various diameters.

The synthesis of GaAs nanowires has been initiated more than 10 years ago with several different methods.[13−19] In this study, GaAs nanowires are synthesized by metal organic chemical vapor deposition (MOCVD) with selective area growth (SAG).[12,20] Trimethylgallium (TMGa), trimethylaluminum (TMAl), and arsine are used as precursors for Ga, Al, and As deposition. High density arrays of GaAs nanowires are grown along the (111) direction on silicon substrates. A thermally grown silicon oxide layer is used as a mask for the SAG growth. A Raith electron beam lithography (EBL) system is used to pattern a 1 mm × 1 mm array of holes with 600 nm pitch. A short (20−30 s) buffered HF etch is performed to expose the crystalline silicon surface before loading the sample into the MOCVD reactor. The sample is first annealed in hydrogen at 920 °C for 5 min to remove the native oxide. Arsine flows while the temperature is cooled from 850 to 440 °C. Nucleations of GaAs are grown at 440 °C for 8 min with partial pressures of 3.74×10^{-7} and 4.78×10^{-5} atm for TMGa and arsine, respectively. After nucleation, the temperature is increased to 790 °C for nanowire growth with the same partial pressures of TMGa and arsine. The growth rate is approximately 8.33 Å/s. Using these conditions, nanowires are grown with very uniform cross section along the length of each nanowire up to 10 μm long. After GaAs nanowire growth, an $Al_xGa_{1-x}As$ layer is deposited as a passivation layer with partial pressures of 3.74×10^{-7}, 4.78×10^{-5}, and 2.18×10^{-7} atm for TMGa, arsine, and TMAl, respectively. An additional thin layer of GaAs (partial pressures of 1.41×10^{-5} atm for TMG and 4.78×10^{-4} atm for arsine) is grown to prevent oxidation of the $Al_xGa_{1-x}As$ shell. For individual nanowire measurements, the nanowires were transferred onto a SiO_2/Si substrate with lithographically defined grid markers, which enables us to record the location of individual nanowires for Raman spectroscopy and photoluminescence mapping.[21] In order to measure the minority carrier diffusion length, the GaAs nanowire was contacted by two metal electrodes using EBL. Before evaporation of the metal contacts, a short oxygen plasma was performed to remove the residual resist and oxidize the outer shell ($Al_xGa_{1-x}As$ and GaAs). The oxidized shell was then removed using a mixture of HCl:H_2O (1:1). Ohmic contacts can be easily obtained between GeAu/Ni/Au metal contacts and bulk GaAs after annealing. GaAs nanowires, however, are completely dissolved in the electrodes at these high annealing temperatures, and the lower annealing temperatures required result in nonlinear, high resistance Schottky contacts.

Micro-Raman spectroscopy and micro-PL mapping are performed using a translation stage with 100 nm step resolution and a high numerical aperture objective lens (100×). A silicon CCD detector is used to detect photoluminescence in the range from 500 to 900 nm and Raman shift from 150 to 3200 cm^{-1}.

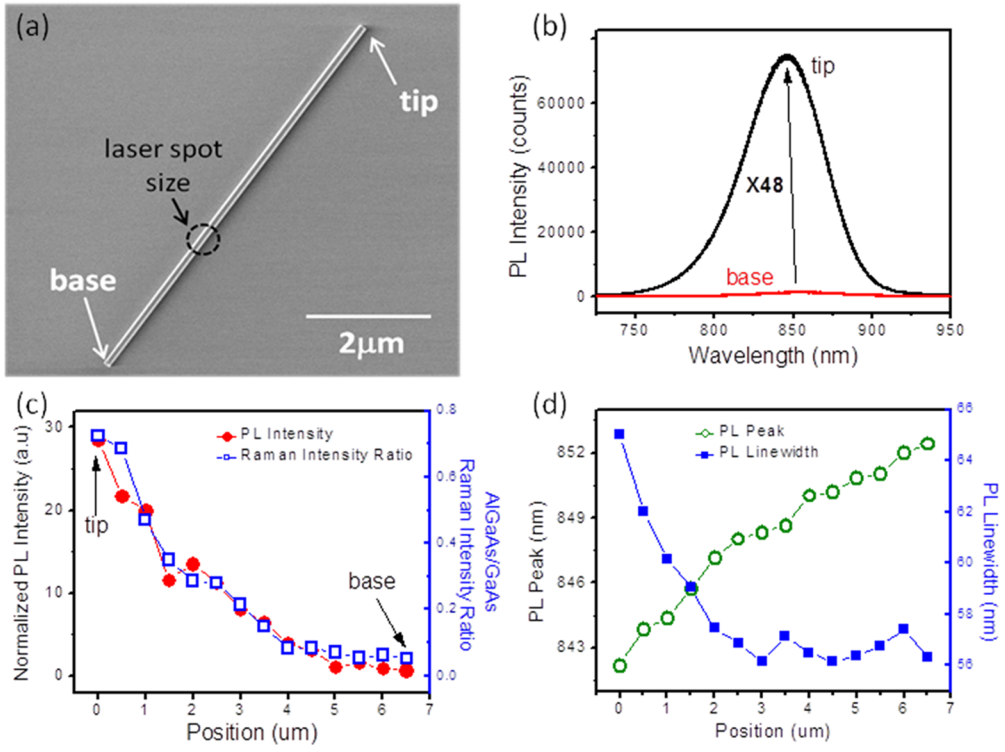

Figure 2. (a) SEM image of a tapered $Al_xGa_{1-x}As$-passivated GaAs nanowire. (b) Continuous-wave PL spectra taken at the tip and base of the nanowire in part a. (c, d) Spatially mapped PL and Raman data along the nanowire axis plotted as a function of position.

dx.doi.org/10.1021/nl301391h | *Nano Lett.* XXXX, XXX, XXX−XXX

Low power (<0.5 mW) excitation by a continuous 532 nm laser is used to avoid optical heating of the nanowires. EBIC measurements are carried out in a JEOL JSM-6610 scanning electron microscope (SEM) equipped with a voltage source (Keithley 2400) and a low noise current preamplifier (Ithaco 1201). In time-resolved PL measurements, sample excitation was carried out with a pump pulse (Tsunami fs laser) of center wavelength 800 nm and pulse energy 32 pJ. The PL signal was detected by a streak camera (Hamamatsu C5680) with an extended response NIR streak tube. The photon collection was centered at 860 nm with a bandwidth of 75 nm. The data integration time was 6000 s, and the minimum system response is 60 ps.

Figure 2a shows a SEM image of a 7 μm long $Al_xGa_{1-x}As$-passivated, undoped GaAs nanowire. The diameter of the nanowire is tapered from the tip to the base of the nanowire due to the inhomogeneity of the $Al_xGa_{1-x}As$ passivation layer. The tapered structure of the passivated nanowires was studied by atomic force microscopy (AFM), as shown in Figure S2 in the Supporting Information, which shows that the $Al_xGa_{1-x}As$ coating varies from 0 to 11 nm in thickness. This thickness variation was also verified by high resolution transmission electron microscopy (HRTEM), as shown in Figure S3 of the Supporting Information. The Raman intensity ratio of the AlAs peaks (337 and 371 cm^{-1}) to that of GaAs (266.5 cm^{-1}) gives a relative measure of the $Al_xGa_{1-x}As$ thickness. This ratio changes from 0.7 at the tip of the nanowire to almost zero (no passivation) at the base, as shown in Figure 2c (right axis). On the basis of these Raman spectra, there is no change in the composition of $Al_xGa_{1-x}As$ along the length of the nanowire. The aluminum composition x can be obtained from the vibrational frequency of the AlAs-like LO Raman mode via the following relation: $\omega_{LO}^{AlAs}(x) = 364.7 + 46.7x - 9.4x^2$.[22,23] On the basis of the Raman spectrum shown in Figure S4 of the Supporting Information, we found a composition of 14.5% aluminum, which is close to the value of 12% characterized by X-ray diffraction measurements presented in a previous publication using similar growth conditions.[19] The PL spectra also show a strong position dependence due to the varying degree of passivation along the length of the nanowire. Figure 2b shows the photoluminescence spectra taken at both ends of the nanowire, which show a 48-fold enhancement in the PL intensity with passivation. Surface states in the less-passivated regions form nonradiative recombination sites causing most of the photoexcited carriers to recombine nonradiatively at the nanowire surface, thereby lowering the PL intensity. On the basis of our previous HRTEM studies,[24] we found that the density of stacking faults is uniform throughout the length of the bare nanowires. Also, since EDX measurements on bare GaAs nanowires show an equal composition of Ga and As throughout the length of these nanowrires, we believe that the large change in PL intensity is mainly due to the $Al_xGa_{1-x}As$ passivation layer. This PL enhancement indicates that these surface states have been successfully passivated by the $Al_xGa_{1-x}As$ layer. In addition to enhancement in the PL intensity, we also observe a blueshift (from 852 to 842 nm) and broadening (from 56 to 65 nm) in the PL emission, as shown in Figure 2d. Strain-induced optical band gap modulation[25] is excluded here in accordance with the spatially mapped Raman data, which do not show any shift in the Raman modes of the GaAs. The GaAs Raman peak remains almost constant at 266.5 cm^{-1} throughout the length of the nanowire. Thus, we attribute the broadening and blueshift to filling of the conduction band with free carriers.[26] Without $Al_xGa_{1-x}As$ passivation, most of the free carriers are depleted in the GaAs core, resulting in band edge-to-band edge PL emission. After the surface states are passivated, free carriers begin filling up the conduction band, causing a blueshift in the PL emission.[26] Since the amount of blueshift depends on the number of free carriers, the inhomogeneity in surface passivation leads to broadening of the PL peak. A similar effect was observed by Titova et al. in InP nanowires, which showed a broadening and blueshift in PL emission under illumination due to the presence of a high-density electron–hole plasma.[27]

Figure 3a shows a SEM image of a GaAs nanowire with a metal (Cr/Au) electrode patterned on top using EBL. The

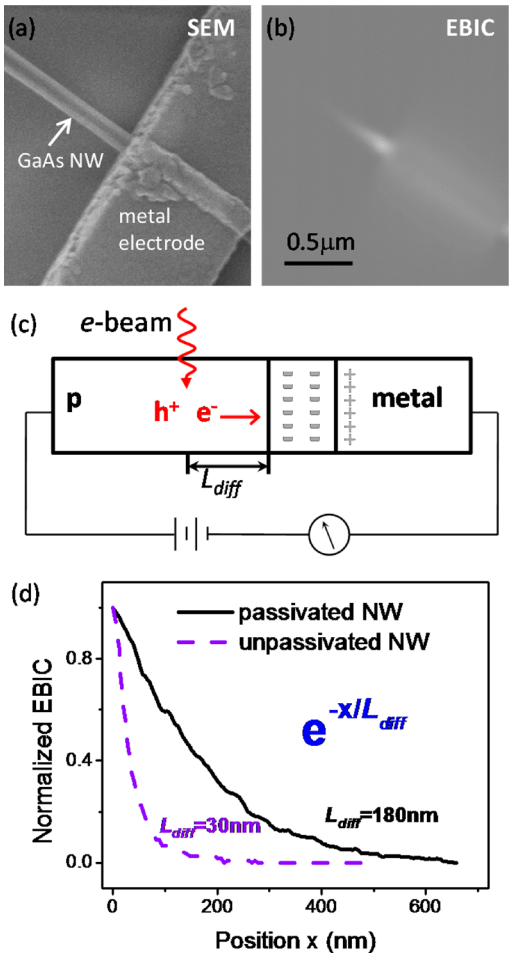

Figure 3. (a) SEM image of an $Al_xGa_{1-x}As$-passivated GaAs nanowire device and (b) corresponding EBIC image. (c) Schematic diagram illustrating the electron beam induced current measurement. (d) EBIC profiles along the nanowire axis for passivated and bare nanowires.

electrode forms a Schottky contact at the nanowire surface, and the current–voltage characteristics show a typical nonlinear behavior. Figure 3c shows a schematic diagram of the EBIC measurement technique, where the focused electron beam creates electron–hole pairs in a p-type nanowire. Electron–hole pairs generated within one minority carrier diffusion length of the metal–semiconductor Schottky junction will, on average, result in a measurable current. Minority carriers generated far away from the Schottky junction will recombine and, therefore, not contribute to the measured (EBIC) current. By spatially mapping the EBIC current, we can determine the

dx.doi.org/10.1021/nl301391h | Nano Lett. XXXX, XXX, XXX–XXX

minority carrier diffusion length directly. Figure 3b shows the EBIC map corresponding to the SEM image in Figure 3a. Here, an acceleration voltage of 5 kV was used to create electron–hole pairs in this measurement. The EBIC signal is strongest near the Schottky interface and gradually diminishes away from the contact. Figure 3d shows the EBIC intensity profile plotted along the nanowire axis. The minority carrier diffusion length, L_{diff}, is extracted by fitting with an exponentially decaying function. For passivated nanowires, we find that L_{diff} = 180 nm, while, for unpassivated nanowires, L_{diff} = 30 nm. This value of 30 nm corresponds to the minimum resolution of our EBIC system. Despite this 6-fold increase in L_{diff} with passivation, 180 nm is a relatively short diffusion length, roughly on the scale of the diameter (90 nm). Dense twin stacking faults have been observed in these nanowires by high resolution transmission electron microscopy (shown in the Supporting Information), which are expected to affect the electron transport. However, the observed L_{diff} = 180 nm is more than 2 orders of magnitude longer than the average separation between twin stacking faults, indicating that they do not form strong centers for electron–hole recombination.

We also perform time-resolved photoluminescence spectroscopy in order to determine the carrier lifetimes in passivated and unpassivated GaAs nanowires. For these measurements, shorter nanowires (1.5 μm) were grown to mitigate the effects associated with nonuniform passivation. This data is shown in Figure 4. For unpassivated nanowires, the PL lifetime is shorter

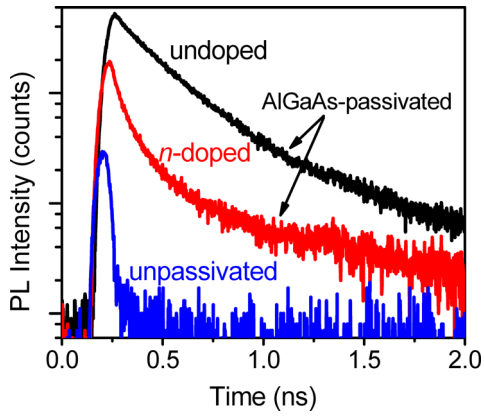

Figure 4. Time-resolved photoluminescence spectra of passivated and unpassivated nanowires with different impurity concentrations.

than the instrument response time of our setup (60 ps). However, passivated nanowires exhibit a significantly longer lifetime due to the passivation of surface states. In addition to the instrument component, two time constants are needed to fit the TRPL curve. The average time constants are 0.2 ns for the short lifetime and 1.3 ns for the long lifetime. Discrepancies between the lifetimes measured in different regions of the nanowire array are due to the inhomogeneous crystal quality and passivation, as has been seen in single nanowire TRPL measurements.[9] In passivated, highly doped nanowires, both the photoluminescence intensity and lifetime significantly decrease due to the increase of impurity scattering, resulting in average time constants of 0.1 and 0.9 ns for the short and long lifetimes, respectively. This data set indicates that, for the doped, passivated nanowires, the minority carrier lifetime is not limited by surface recombination, since the doped nanowire exhibits a shorter PL lifetime than the undoped nanowire.

On the basis of the measured carrier lifetimes determined from TRPL, the surface recombination velocity S can be estimated by the following equation[28,29]

$$\frac{1}{\tau} = \frac{1}{\tau_b} + \frac{4S}{d}$$

where τ is the effective carrier lifetime, τ_b is the carrier lifetime in bulk material, and d is the diameter of the GaAs core (90 nm). Using a bulk carrier lifetime of τ_b = 1.3 μs, we calculate the surface recombination velocity S to be 1.7×10^3 and 1.1×10^4 cm·s^{-1} for the long and short decay constants.[3] For bulk GaAs with appropriate passivation, SRV values as low as 500 have been reported.[30] The relatively high SRV values observed in the nanowire samples indicate that either the surface states have only been partially passivated or stacking faults and bulk impurities are limiting the SRV.[3] This is confirmed by the highly doped nanowires, which show a significantly reduced PL lifetime compared to the corresponding undoped sample. The minority carrier lifetime and surface recombination velocity (SRV) of twin-free $Al_xGa_{1-x}As$ passivated GaAs nanowires grown by the vapor–liquid–solid (VLS) growth method were reported by three other groups ranging from 1 to 2.5 ns and around 3×10^3 cm/s, respectively.[8,9,31,32] While dense twin stacking faults are normally seen in our nanowires, using catalyst-free selective area MOCVD growth, we did not observe a significant difference in the lifetime and SRV compared to the numbers reported in twin-free nanowires. This indicates that these twin stacking faults are not the main factor limiting minority carrier dynamics. We can also correlate L_{diff} with τ to estimate the minority carrier mobility μ by the following equation

$$L_{diff} = \sqrt{D\tau}$$

where the diffusion coefficient is given by $D = \mu \cdot kT/e$ and both L_{diff} and τ are measured at room temperature. The short and long decay constants give higher and lower limits of the minority carrier mobility μ to be 67.5 and 10.3 cm^2 V^{-1} s^{-1}, respectively, for the passivated nanowires. These mobilities are far lower than the values in bulk GaAs, which have been both experimentally and theoretically reported in the range from 1000 to 7500 cm^2 V^{-1} s^{-1} depending on the acceptor concentration.[33,34]

In conclusion, a systematic study of $Al_xGa_{1-x}As$-passivated GaAs nanowires shows the significance of surface passivation on free carrier dynamics in GaAs nanowires. Weak PL emission and short PL lifetimes are observed in bare (unpassivated) GaAs nanowires. We observe a 48-fold enhancement in the PL intensity and a 6-fold increase in the minority carrier diffusion length with surface passivation. The surface recombination velocity is calculated to lie in the range from 1.7×10^3 to 1.1×10^4 cm·s^{-1}. For the passivated nanowires, we estimate the minority carrier mobility to lie in the range from 10.3 to 67.5 cm^2 V^{-1} s^{-1}, based on the measured lifetimes and diffusion length. Furthermore, the relatively long minority carrier diffusion lengths indicate that twin stacking faults do not limit the minority carrier lifetimes in passivated nanowires.

■ ASSOCIATED CONTENT

Supporting Information

Additional figures showing GaAs nanowires grown on different substrates, the diameter of GaAs nanowires as a function of position and AFM height profiles at different positions, TEM

dx.doi.org/10.1021/nl301391h | Nano Lett. XXXX, XXX, XXX–XXX

and HRTEM images, EDX and Raman spectra, and current-voltage curves. This material is available free of charge via the Internet at http://pubs.acs.org.

AUTHOR INFORMATION

Corresponding Author

*Address: Department of Electrical Engineering, University of Southern California, Powell Hall of Engineering, PHE 624, Los Angeles, CA 90089-0271. Phone: 213-740-8787. E-mail: scronin@usc.edu.

Notes

The authors declare no competing financial interest.

ACKNOWLEDGMENTS

This material is based upon work supported as part of the Center for Energy Nanoscience (CEN), an Energy Frontier Research Center (EFRC) funded by the U.S. Department of Energy, Office of Science and Office of Basic Energy Sciences, under Award DE-SC0001013. The portion of the work done at the Aerospace Corporation was funded by the independent research and development program at the Aerospace Corporation.

REFERENCES

(1) Tomioka, K.; Motohisa, J.; Hara, S.; Hiruma, K.; Fukui, T. GaAs/AlGaAs Core Multishell Nanowire-Based Light-Emitting Diodes on Si. *Nano Lett.* **2010**, *10* (5), 1639−1644.

(2) Geisz, J. F.; Kurtz, S.; Wanlass, M. W.; Ward, J. S.; Duda, A.; Friedman, D. J.; Olson, J. M.; McMahon, W. E.; Moriarty, T. E.; Kiehl, J. T. High-efficiency GaInP/GaAs/InGaAs triple-junction solar cells grown inverted with a metamorphic bottom junction. *Appl. Phys. Lett.* **2007**, *91* (2), 023502-3.

(3) Nelson, R. J.; Sobers, R. G. Minority-carrier lifetimes and internal quantum efficiency of surface-free GaAs. *J. Appl. Phys.* **1978**, *49* (12), 6103−6108.

(4) Lloyd-Hughes, J.; Merchant, S. K. E.; Fu, L.; Tan, H. H.; Jagadish, C.; Castro-Camus, E.; Johnston, M. B. Influence of surface passivation on ultrafast carrier dynamics and terahertz radiation generation in GaAs. *Appl. Phys. Lett.* **2006**, *89* (23), 232102-3.

(5) Katzenmeyer, A. M.; Léonard, F. o.; Talin, A. A.; Wong, P.-S.; Huffaker, D. L. Poole−Frenkel Effect and Phonon-Assisted Tunneling in GaAs Nanowires. *Nano Lett.* **2010**, *10* (12), 4935−4938.

(6) Suyatin, D. B.; Thelander, C.; Björk, M. T.; Maximov, I.; Samuelson, L. Sulfur passivation for ohmic contact formation to InAs nanowires. *Nanotechnology* **2007**, *18*, 105307.

(7) Sheldon, M. T.; Eisler, C. N.; Atwater, H. A. GaAs Passivation with Trioctylphosphine Sulfide for Enhanced Solar Cell Efficiency and Durability. *Adv. Energy Mater.* **2012**, *2* (3), 339−344.

(8) Demichel, O.; Heiss, M.; Bleuse, J.; Mariette, H.; Fontcuberta i Morral, A. , Impact of surfaces on the optical properties of GaAs nanowires. *Appl. Phys. Lett.* **2010**, *97* (20), 201907-3.

(9) Perera, S.; Fickenscher, M. A.; Jackson, H. E.; Smith, L. M.; Yarrison-Rice, J. M.; Joyce, H. J.; Gao, Q.; Tan, H. H.; Jagadish, C.; Zhang, X.; Zou, J. Nearly intrinsic exciton lifetimes in single twin-free GaAs/AlGaAs core-shell nanowire heterostructures. *Appl. Phys. Lett.* **2008**, *93* (5), 053110-3.

(10) Parkinson, P.; Joyce, H. J.; Gao, Q.; Tan, H. H.; Zhang, X.; Zou, J.; Jagadish, C.; Herz, L. M.; Johnston, M. B. Carrier Lifetime and Mobility Enhancement in Nearly Defect-Free Core−Shell Nanowires Measured Using Time-Resolved Terahertz Spectroscopy. *Nano Lett.* **2009**, *9* (9), 3349−3353.

(11) Ouattara, L.; Mikkelsen, A.; Sköld, N.; Eriksson, J.; Knaapen, T.; Ćavar, E.; Seifert, W.; Samuelson, L.; Lundgren, E. GaAs/AlGaAs Nanowire Heterostructures Studied by Scanning Tunneling Microscopy. *Nano Lett.* **2007**, *7* (9), 2859−2864.

(12) Tomioka, K.; Kobayashi, Y.; Motohisa, J.; Hara, S.; Fukui, T. Selective-area growth of vertically aligned GaAs and GaAs/AlGaAs core−shell nanowires on Si(111) substrate. *Nanotechnology* **2009**, *20*, 145302.

(13) Trentler, T. J.; Hickman, K. M.; Goel, S. C.; Viano, A. M.; Gibbons, P. C.; Buhro, W. E. Solution-Liquid-Solid Growth of Crystalline III-V Semiconductors: An Analogy to Vapor-Liquid-Solid Growth. *Science* **1995**, *270* (5243), 1791−1794.

(14) Duan, X.; Lieber, C. M. General Synthesis of Compound Semiconductor Nanowires. *Adv. Mater.* **2000**, *12* (4), 298−302.

(15) Duan, X.; Wang, J.; Lieber, C. M. Synthesis and optical properties of gallium arsenide nanowires. *Appl. Phys. Lett.* **2000**, *76* (9), 1116−1118.

(16) Lee, H. G.; Jeon, H. C.; Kang, T. W.; Kim, T. W. Gallium arsenide crystalline nanorods grown by molecular-beam epitaxy. *Appl. Phys. Lett.* **2001**, *78* (21), 3319−3321.

(17) Shi, W. S.; Zheng, Y. F.; Wang, N.; Lee, C. S.; Lee, S. T. A General Synthetic Route to III−V Compound Semiconductor Nanowires. *Adv. Mater.* **2001**, *13* (8), 591−594.

(18) Shi, W. S.; Zheng, Y. F.; Wang, N.; Lee, C. S.; Lee, S. T. Oxide-assisted growth and optical characterization of gallium-arsenide nanowires. *Appl. Phys. Lett.* **2001**, *78* (21), 3304−3306.

(19) Noborisaka, J.; Motohisa, J.; Hara, S.; Fukui, T. Fabrication and characterization of freestanding GaAs/AlGaAs core-shell nanowires and AlGaAs nanotubes by using selective-area metalorganic vapor phase epitaxy. *Appl. Phys. Lett.* **2005**, *87* (9), 093109-3.

(20) Chu, H.-J.; Yeh, T.-W.; Stewart, L.; Dapkus, P. D. Wurtzite InP nanowire arrays grown by selective area MOCVD. *Phys. Status Solidi C* **2010**, *7* (10), 2494−2497.

(21) Chang, C.-C.; Chen, H.; Chen, C.-C.; Hung, W.-H.; Hsu, I.-K.; Theiss, J.; Zhou, C.; Cronin, S. B. Tailoring the crystal structure of individual silicon nanowires by polarized laser annealing. *Nanotechnology* **2011**, *22*, 305709.

(22) Solomon, G. S.; Kirillov, D.; Chui, H. C.; Harris, J. S. Determination of AlAs mole fraction in $Al_xGa_{1-x}As$ using Raman spectroscopy and x-ray diffraction. *J. Vac. Sci. Technol., B* **1994**, *12*, 1078−1081.

(23) Wasilewski, Z. R.; Dion, M. M.; Lockwood, D. J.; Poole, P.; Streater, R. W.; SpringThorpe, A. J. Composition of AlGaAs. *J. Appl. Phys.* **1997**, *81* (4), 1683−1694.

(24) Madaria, A. R.; Yao, M.; Chi, C.; Huang, N.; Lin, C.; Li, R.; Povinelli, M. L.; Dapkus, P. D.; Zhou, C. Toward Optimized Light Utilization in Nanowire Arrays Using Scalable Nanosphere Lithography and Selected Area Growth. *Nano Lett.* **2012**, *12* (6), 2839−2845.

(25) Montazeri, M.; Fickenscher, M.; Smith, L. M.; Jackson, H. E.; Yarrison-Rice, J.; Kang, J. H.; Gao, Q.; Tan, H. H.; Jagadish, C.; Guo, Y.; Zou, J.; Pistol, M.-E.; Pryor, C. E. Direct Measure of Strain and Electronic Structure in GaAs/GaP Core−Shell Nanowires. *Nano Lett.* **2010**, *10* (3), 880−886.

(26) De-Sheng, J.; Makita, Y.; Ploog, K.; Queisser, H. J. Electrical properties and photoluminescence of Te-doped GaAs grown by molecular beam epitaxy. *J. Appl. Phys.* **1982**, *53* (2), 999−1006.

(27) Titova, L. V.; Hoang, T. B.; Yarrison-Rice, J. M.; Jackson, H. E.; Kim, Y.; Joyce, H. J.; Gao, Q.; Tan, H. H.; Jagadish, C.; Zhang, X.; Zou, J.; Smith, L. M. Dynamics of Strongly Degenerate Electron−Hole Plasmas and Excitons in Single InP Nanowires. *Nano Lett.* **2007**, *7* (11), 3383−3387.

(28) Demichel, O.; Calvo, V.; Besson, A.; Noé, P.; Salem, B.; Pauc, N.; Oehler, F.; Gentile, P.; Magnea, N. Surface Recombination Velocity Measurements of Efficiently Passivated Gold-Catalyzed Silicon Nanowires by a New Optical Method. *Nano Lett.* **2010**, *10* (7), 2323−2329.

(29) Dan, Y.; Seo, K.; Takei, K.; Meza, J. H.; Javey, A.; Crozier, K. B. Dramatic Reduction of Surface Recombination by in Situ Surface Passivation of Silicon Nanowires. *Nano Lett.* **2011**, *11* (6), 2527−2532.

(30) Nelson, R. J.; Sobers, R. G. Interfacial recombination velocity in GaAlAs/GaAs heterostructures. *Appl. Phys. Lett.* **1978**, *32* (11), 761−763.

(31) Joyce, H. J.; Gao, Q.; Tan, H. H.; Jagadish, C.; Kim, Y.; Zhang, X.; Guo, Y.; Zou, J. Twin-Free Uniform Epitaxial GaAs Nanowires Grown by a Two-Temperature Process. *Nano Lett.* **2007**, *7* (4), 921−926.
(32) Breuer, S.; Pfüller, C.; Flissikowski, T.; Brandt, O.; Grahn, H. T.; Geelhaar, L.; Riechert, H. Suitability of Au- and Self-Assisted GaAs Nanowires for Optoelectronic Applications. *Nano Lett.* **2011**, *11* (3), 1276−1279.
(33) Walukiewicz, W.; Lagowski, J.; Jastrzebski, L.; Gatos, H. C. Minority-carrier mobility in p-type GaAs. *J. Appl. Phys.* **1979**, *50* (7), 5040−5042.
(34) Harmon, E. S.; Lovejoy, M. L.; Melloch, M. R.; Lundstrom, M. S.; de Lyon, T. J.; Woodall, J. M. Experimental observation of a minority electron mobility enhancement in degenerately doped p-type GaAs. *Appl. Phys. Lett.* **1993**, *63* (4), 536−538.

dx.doi.org/10.1021/nl301391h | *Nano Lett.* XXXX, XXX, XXX−XXX